The Emergent Simplicity of Galaxy Size

Andrew Hearin[1], Peter Behroozi[2], Andrey Kravtsov[3], Benjamin Moster[4]

[1] *Argonne National Laboratory, Argonne, IL, USA 60439, USA*
[2] *Department of Physics, University of Arizona, 1118 E 4th St, Tucson, AZ 85721 USA*
[3] *Department of Astronomy & Astrophysics, The University of Chicago, Chicago, IL 60637 USA*
[4] *Universitäts-Sternwarte, Ludwig-Maximilians-Universität München, Scheinerstr. 1, 81679 München, Germany*

29 September 2017

ABSTRACT

We derive empirical modeling constraints on the connection between dark matter halos and the half-light radius of galaxies, $R_{1/2}$. Novel to this work, we study galaxy size using new SDSS measurements of the $R_{1/2}-$dependence of galaxy clustering. Smaller galaxies cluster stronger relative to larger galaxies of the same stellar mass, a new result. We show that this clustering signal is largely driven by centrals being larger than satellite galaxies of the same halo mass. We use `Halotools` to build a forward model of galaxy size in which $R_{1/2}$ is set by the halo virial radius $R_{\rm vir}$ at the time the halo reaches its peak mass, with scatter in $R_{1/2}$ that is strongly correlated with the halo scale radius $R_{\rm s}$ at that time. The $R_{1/2}-$dependent clustering of this model is strikingly similar to our SDSS measurements in magnitude, scale-dependence, and M_*-dependence. Together with the result that stellar mass stripping of satellites has only a mild impact on $R_{1/2}-$dependent clustering, this suggests that the relative size of centrals and satellites is already in place at the time of satellite infall, and supports the notion that L_* galaxy and halo profiles co-evolve across many Gyr of cosmic time. Our results can be treated as a boundary condition for more complex and fine-grained models of galaxy size, and provide a simple means for cosmological surveys to generate synthetic galaxy populations with realistic sizes across the cosmic web.

1 INTRODUCTION

Some introduction goes here.

2 DATA AND SIMULATIONS

Our galaxy sample comes from the catalog of SDSS galaxy profile decompositions provided by Meert et al. (2015). This catalog is based on Data Release 10 of the Sloan Digital Sky Survey (SDSS, Ahn et al. 2014), with improvements to the photometry pipeline and light profile fitting methods (Vikram et al. 2010; Bernardi et al. 2013, 2014; Meert et al. 2013). In the version of this catalog that we use, two-dimensional $r-$band profiles were fit with a two-component de Vaucouleurs + exponential profile to determine the half-light radius $R_{1/2}$. We apply the Bell et al. (2003) mass-to-light ratio to the $r-$band flux and $g-r$ colors in this catalog to obtain an estimate for the total stellar mass M_* of every galaxy. We calculate two-point clustering $w_{\rm p}$ of our SDSS galaxy sample using line-of-sight projection of $\pi_{\rm max} = 20{\rm Mpc}$ using the `correl` program in `UniverseMachine`.

As the bedrock of our modeling, we use the catalog of `Rockstar` subhalos identified at $z = 0$ in the Bolshoi-Planck simulation (Klypin et al. 2011; Behroozi et al. 2013,?; Riebe et al. 2013; Rodríguez-Puebla et al. 2016). The particular version of the catalog we use is made publicly available through `Halotools` (Hearin et al. 2016), with `version_name` = 'halotools_v0p4'.

We additionally explore the potential existence of satellite galaxies that reside in subhalos that are not identified by halo-finder to the present day, so-called "orphan galaxies" (see, e.g., Campbell et al. 2017). We use an extension of `Consistent Trees` that models the evolution of subhalos after disruption. The phase space evolution of orphans is approximated by following a point mass evolving in the host halo potential according to the orbital parameters of the subhalo at the time of disruption; the evolution of subhalo mass and circular velocity is approximated using the semi-analytic model presented in Jiang & van den Bosch (2014).

For mock galaxies, to compute galaxy clustering we employ the distant observer approximation by treating the simulation $z-$axis as the line-of-sight. We compute $w_{\rm p}$ using the `mock_observables.wp` function in `Halotools`, which is a python implementation of the algorithm in the `Corrfunc` C library (Sinha & Garrison 2017).

All numerical values of $R_{1/2}$ will be quoted in physical kpc, and all values of M_* and $M_{\rm halo}$ in $M_\odot$, assuming

$H_0 = 67.8$ km/s $\equiv 100h$ km/s, the best-fit value from Planck Collaboration et al. (2016). To scale stellar masses to "$h = 1$ units" (Croton 2013), our numerically quoted values for M_* should be multiplied by a factor of h^2, while our halo masses and distances should be multiplied by a factor of h.

3   GALAXY-HALO MODEL

3.1   Stellar mass model

We map M_* onto subhalos with the best-fit stellar-to-halo mass relation from Moster et al. (2013):

$$\langle M_*/M_{\rm halo} \rangle = 2N \left[(M_{\rm halo}/M_1)^{-\beta} + (M_{\rm halo}/M_1)^{\gamma} \right]^{-1}. \tag{1}$$

For halo mass $M_{\rm halo}$ we use $M_{\rm peak}$, the largest value of $M_{\rm vir}$ ever attained along the main progenitor branch of the subhalo.

The values of the best-fit parameters in Moster et al. (2013) were fit to a stellar mass function (SMF) with values $M_*^{\rm MPA-JHU}$ based on the MPA-JHU catalog (Kauffmann et al. 2003; Brinchmann et al. 2004), which differs from the SMF in our galaxy sample (see, e.g., Bernardi et al. 2014). We account for this difference by manually tabulating the median value $\langle M_*^{\rm Meert+15} | M_*^{\rm MPA-JHU} \rangle$ in logarithmic bins spanning $9 < \log_{10} M_*^{\rm MPA-JHU}/M_\odot < 12$, and applying the median correction to the Monte Carlo realization of the mock galaxy sample. This results in a typical boost of ~ 0.25 dex at $M_*^{\rm MPA-JHU} \approx 10^{9.75} M_\odot$, and ~ 0.4 dex at $M_*^{\rm MPA-JHU} \approx 10^{11.5} M_\odot$.

3.2   Galaxy size models

In §4, we calculate predictions for the $R_{1/2}$−dependence of galaxy clustering for several different kinds of empirical models, described in turn below.

3.2.1   K13 model

In Kravtsov (2013), it was found that if a stellar-to-halo mass relation is inverted to map halo mass estimates $M_{\rm halo}$ onto SDSS galaxies, and then the $M_{\rm halo} - R_{\rm vir}$ relation is applied to map values of $R_{\rm vir}$ onto the galaxies, then the resulting $R_{1/2} - R_{\rm vir}$ relation of SDSS galaxies exhibits the following linear scaling across a wide range of stellar mass:

$$R_{1/2} = 0.0125 R_{\rm vir} \tag{2}$$

Motivated by the simplicity of this scaling relation, we transform the Kravtsov (2013) into a forward model using `Halotools`. For the virial radius of halos and subhalos, we use $R_{\rm M_{peak}}$, the value of $R_{\rm vir}$ in physical units of kpc measured at the time of peak subhalo mass, defined by

$$M_{\rm peak} \equiv \frac{4\pi}{3} R_{\rm M_{peak}}^3 \Delta_{\rm vir}(z_{\rm peak}) \rho_{\rm m}(z_{\rm peak}) \tag{3}$$

When generating predictions for the K13 model galaxy sizes, we add uncorrelated log-normal scatter of $\sigma_{\rm R_{1/2}} =$

0.2 dex to generate a Monto Carlo realization of the model population.

3.2.2   K13 + co-evolution model

The *K13 + co-evolution model* model is identical to K13, but the scatter in $R_{1/2}$ at fixed $R_{\rm M_{peak}}$ is no longer purely stochastic, but is instead correlated with $V_{\rm peak}$. We implement scatter correlations using the `halotools.empirical_models.conditional_abunmatch` function, which generalizes the Conditional Abundance Matching technique described in Hearin et al. (2014).

3.2.3   K13 + stripping model

We will also consider models for galaxy size in which stellar mass is stripped from satellite galaxies after infall. The basis of this class of models is the fitting function presented in Smith et al. (2016), which was calibrated by studying stellar mass loss in a suite of high-resolution hydrodynamical simulations. In this model, f_* quantifies the fraction of stellar mass lost as a function of $f_{\rm DM}$, the amount of dark matter that has been stripped since infall:

$$f_* = 1 - \exp(-14.2 f_{\rm DM}) \tag{4}$$

For $f_{\rm DM}$ we use the ratio of present-day subhalo mass divided by the peak mass, $M_{\rm vir}/M_{\rm peak}$. If we denote the post-stripping stellar mass as M_*', then we have $M_*' \equiv f_* M_*$, where M_* is given by Eq. 1. We then calculate the post-stripping radius by interpolating $\langle R_{1/2}' | M_*' \rangle$ directly from SDSS data.

4   RESULTS

In §4.1 we show comparisons between the galaxy size model described in §3 and our SDSS sample.

4.1   Testing Model Predictions

In Figure 1 we show the scaling of galaxy size $R_{1/2}$ with M_*. Scattered gray points show the scaling relation for our SDSS galaxy sample, while the black curve shows the median relation $\langle R_{1/2} | M_* \rangle$ implied by the model described in §3.

In Figure 2 we present new measurements of the $R_{1/2}$−dependence of projected galaxy clustering, $w_{\rm p}(r_{\rm p})$. Because galaxy clustering has well-known dependence upon M_* that is not the subject of this work, we wish to remove this influence and focus purely on the relationship between $R_{1/2}$ and $w_{\rm p}(r_{\rm p})$. To do so, we determine the value $\langle R_{1/2} | M_* \rangle$ by computing a sliding median of $R_{1/2}$, calculated using a window of width $N_{\rm gal} = 1000$. Each galaxy is categorized as either "large" or "small" according to whether it is above or below the median value appropriate for its stellar mass. For any M_*−threshold sample, the SMF of the "large" and "small" subsamples are identical, by construction.
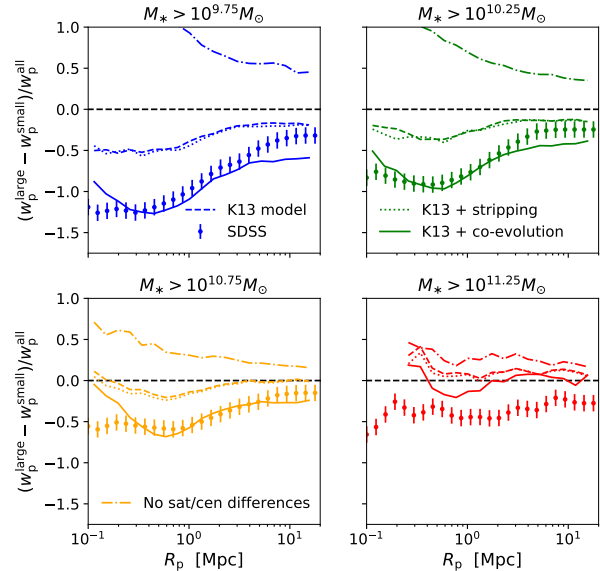
We measure $w_{\rm p}(r_{\rm p})$ separately for large and small subsamples for four different M_* thresholds, $M_* >$
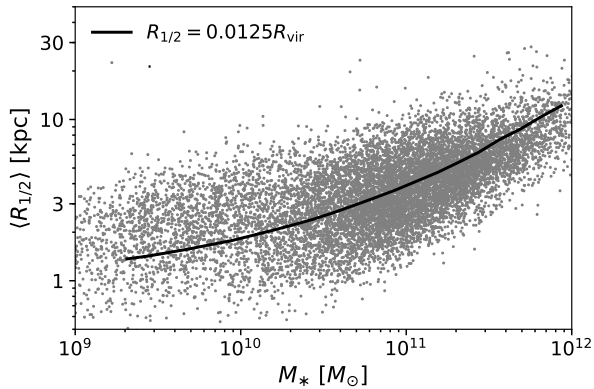
Figure 1. One-point data used to fit the fiducial model. Scattered points show the $R_{1/2} - M_*$ relation for SDSS galaxies as measured in Meert et al. (2015). The black curve shows the median $R_{1/2} - M_*$ relation implied by the model described in §3, in which $R_{1/2} = 0.0125 R_{\rm vir}$. This figure confirms the findings in Kravtsov (2013) that a linear relationship between $R_{\rm vir}$ and $R_{1/2}$, convolved against the nonlinear relationships between $R_{\rm vir}, M_{\rm halo}$ and M_*, correctly predicts the characteristic curvature in the relation $\langle R_{1/2}|M_*\rangle$ over a wide range in stellar mass.

Figure 2. $R_{1/2}-$**dependence of galaxy clustering.** Points with error bars show new SDSS measurements of the $R_{1/2}-$dependence of projected galaxy clustering, $w_{\rm p}$, compared to predictions by the model tuned to the measurements shown in Fig. 1. We define a galaxy as "large" or "small" according to whether it is above or below the median size for its stellar mass, so that in each panel, the SMF of the "large" and "small" subsamples are identical, as described in the text. The y-axis shows *clustering strength ratios,* so that, for example, a y-axis value of -0.5 corresponds to small galaxies being 50% more strongly clustered than large galaxies of comparable stellar mass. Each panel shows results separately for a different volume-limited M_*-threshold samples. See §3.2 for a description of each model.

$10^{9.75} M_\odot$, $M_* > 10^{10.25} M_\odot$, $M_* > 10^{10.75} M_\odot$, and $M_* > 10^{11.25} M_\odot$. We make the same measurements for each volume-limited M_*-threshold sample *without* splitting on size, giving us measurements $w_{\rm p}^{\rm all}, w_{\rm p}^{\rm large}$, and $w_{\rm p}^{\rm small}$ for each threshold sample. This allow us to compute the ratio $(w_{\rm p}^{\rm large} - w_{\rm p}^{\rm small})/w_{\rm p}^{\rm all}$, which we refer to as *the $R_{1/2}$ clustering ratio*. These ratios are the measurements appearing on the y-axis in each panel of Figure 2. Points with error bars show SDSS measurements, solid curves show the clustering ratios of model galaxies as predicted by the model described in §3. Before unpacking the information contained in these clustering measurements, we stress that the good agreement shown between model and data in Figure 2 is a genuine model prediction, since the model parameters were taken directly from Kravtsov (2013), which were fit to the one-point measurements in Fig. 1, whereas the two-point measurements appearing in Figure 2 have heretofore never been measured.

The salient feature of the clustering ratio measurements is that they are negative: small galaxies cluster more strongly than large galaxies of the same stellar mass, a new result. This feature also holds true for model galaxies. This result may be surprising, since $R_{1/2} \propto R_{\rm vir}$, halo mass $R_{\rm vir} \propto M_{\rm halo}^{1/3}$, and clustering strength increases with $M_{\rm vir}$. Based on this simple argument, one would expect the opposite trend to the measurements shown here. We present a resolution to this puzzle in the following section.

4.2 Origin of the size-dependence of galaxy clustering

5 DISCUSSION

5.1 Progression from Backwards to Forwards Modeling

5.2 Implications for Satellite Mass Loss

5.3 Future Directions for Empirical Modeling of Morphology
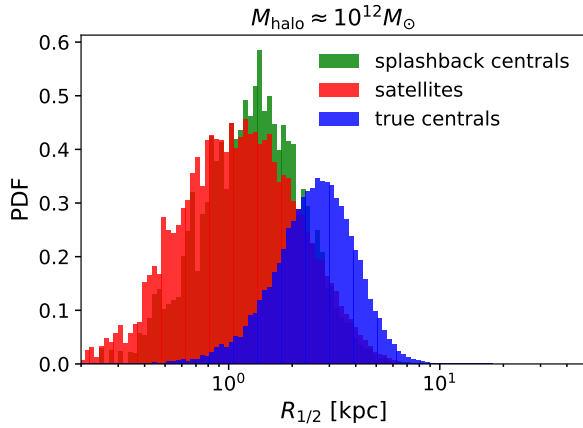
6 CONCLUSIONS

6.1 Summary

ACKNOWLEDGMENTS

REFERENCES

Ahn C. P., Alexandroff R., Allende Prieto C., Anders F., Anderson S. F., Anderton T., Andrews B. H., Aubourg É., Bailey S., Bastien F. A., et al. 2014, ApJS , 211, 17

Behroozi P. S., Wechsler R. H., Wu H.-Y., 2013, ApJ , 762, 109

Figure 3. Relative sizes of centrals and satellites. In a narrow bin of halo mass $M_{\rm halo} = M_{\rm peak} \approx 10^{12} M_\odot$, we show the distribution of model galaxy sizes for different subpopulations galaxies. The red histogram shows the sizes of satellites; the blue histogram shows host halos that have never passed inside the virial radius of a larger halo ("true centrals"); the green histogram host halos that were subhalos inside a larger at some point in their past history ("splashback halos"). In the fiducial model, galaxy size is set by the physical size of the virial radius at the time the (sub)halo attains its peak mass, naturally resulting in smaller sizes for satellites and backsplash centrals relative to true centrals of the same $M_{\rm peak}$.
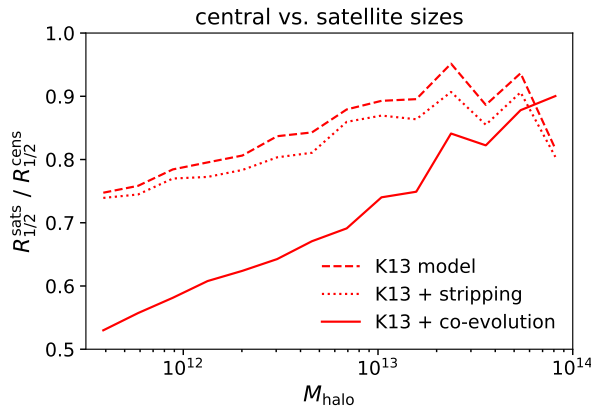
Figure 4. Origin of the $R_{1/2}$−dependence of clustering. Here we compare our fiducial model, in which satellite galaxy size is set by $R_{\rm vir}$ at the time of infall, to a set of alternative models created by shuffling the sizes of various subsamples of the fiducial mock.

Behroozi P. S., Wechsler R. H., Wu H.-Y., Busha M. T., Klypin A. A., Primack J. R., 2013, ApJ , 763, 18

Bell E. F., McIntosh D. H., Katz N., Weinberg M. D., 2003, ApJS , 149, 289

Bernardi M., Meert A., Sheth R. K., Vikram V., Huertas-Company M., Mei S., Shankar F., 2013, MN-RAS , 436, 697

Bernardi M., Meert A., Vikram V., Huertas-Company M., Mei S., Shankar F., Sheth R. K., 2014, MNRAS , 443, 874

Brinchmann J., Charlot S., White S. D. M., Tremonti C., Kauffmann G., Heckman T., Brinkmann J., 2004, MNRAS , 351, 1151

Campbell D., van den Bosch F. C., Padmanabhan N., Mao Y.-Y., Zentner A. R., Lange J. U., Jiang F., Villarreal A., 2017, ArXiv:1705.06347

Croton D. J., 2013, PASA, 30, e052

Hearin A., Campbell D., Tollerud E., et al., 2016, ArXiv e-prints

Hearin A. P., Watson D. F., Becker M. R., Reyes R., Berlind A. A., Zentner A. R., 2014, MNRAS , 444, 729

Jiang F., van den Bosch F. C., 2014, ArXiv e-prints

Kauffmann G., Heckman T. M., White S. D. M., et al., 2003, MNRAS , 341, 33

Klypin A. A., Trujillo-Gomez S., Primack J., 2011, ApJ , 740, 102

Kravtsov A. V., 2013, ApJL , 764, L31

Meert A., Vikram V., Bernardi M., 2013, MNRAS , 433, 1344

Meert A., Vikram V., Bernardi M., 2015, MNRAS , 446, 3943

Moster B. P., Naab T., White S. D. M., 2013, MNRAS , 428, 3121

Planck Collaboration Ade P. A. R., Aghanim N., Arnaud M., Ashdown M., Aumont J., Baccigalupi C., Banday A. J., Barreiro R. B., Bartlett J. G., et al. 2016, AAP, 594, A13

Riebe K., Partl A. M., Enke H., Forero-Romero J., Gottlöber S., Klypin A., Lemson G., Prada F., Primack J. R., Steinmetz M., Turchaninov V., 2013, Astronomische Nachrichten, 334, 691

Rodríguez-Puebla A., Behroozi P., Primack J., Klypin A., Lee C., Hellinger D., 2016, MNRAS , 462, 893

Sinha M., Garrison L., , 2017, Corrfunc: Blazing fast correlation functions on the CPU, Astrophysics Source Code Library

Smith R., Choi H., Lee J., Rhee J., Sanchez-Janssen R., Yi S. K., 2016, ApJ , 833, 109

Vikram V., Wadadekar Y., Kembhavi A. K., Vijayagovindan G. V., 2010, MNRAS , 409, 1379